JOURNAL OF GEOPHYSICAL RESEARCH, VOL. 91, NO. B5, PAGES 4730-4744, APRIL 10, 1986

DYNAMIC COMPRESSION AND VOLATILE RELEASE OF CARBONATES

James A. Tyburczy and Thomas J. Ahrens

Seismological Laboratory, California Institute of Technology, Pasadena

Abstract. Particle velocity profiles upon shock compression and adiabatic release were measured for polycrystalline calcite (Solenhofen limestone) to 12-24 GPa and for porous calcite (Dover chalk, $\rho_o = 1.40$ g/cm^3, 49% porosity) to between 5 and 11 GPa. The electromagnetic particle velocity gauge method was used. Upon shock compression of Solenhofen limestone, the Hugoniot elastic limit was determined to vary from 0.36 to 0.45 GPa. Transition shocks at between 2.5 and 3.7 GPa, possibly arising from the calcite II-III transition, were observed. For the Solenhofen limestone, the release paths lie relatively close to the Hugoniot. Evidence for the occurrence of the calcite III-II transition upon release was observed, but no rarefaction shocks were detected. Initial release wave speeds suggest retention of shear strength up to at least 20 GPa, with a possible loss of shear strength at higher pressures. The measured equation of state is used to predict the fraction of material devolatilized upon adiabatic release as a function of shock pressure. The effect of ambient partial pressure of CO_2 on the calculations is demonstrated. P_{CO_2} should be taken into account in models of atmospheric evolution by means of impact-induced mineral devolatilization. Mass fractions of CO_2 released expected on the basis of a continuum model are much lower than determined experimentally. This discrepancy, and radiative characteristics of shocked calcite, indicate that localization of thermal energy (shear banding) occurs under shock compression even though no solid-solid transitions occur in this pressure range. Release adiabatic data indicate that Dover chalk loses its shear strength when shocked to 10 GPa pressure. At 5 GPa the present data are ambiguous regarding shear strength. For Dover chalk, continuum shock entropy calculations result in a minimum estimate of 90% devolatilization upon complete release from 10 GPa. For calcite, isentropic release paths from calculated continuum Hugoniot temperatures cross into the CaO (solid) + CO_2 (vapor) field at improbably low pressures (for example, 10^{-7} GPa for a shock pressure of 25 GPa). However, calculated isentropic release paths originating from PT points corresponding to previous color temperature under shock measurements cross into the melt plus vapor field at pressures greater than 0.5 GPa, suggesting that devolatilization is initiated at the shear banding sites.

Introduction

The shock compression and release behavior of carbonates is of interest in the study of cratering mechanics, shock metamorphism in carbonate terranes, and the generation of CO_2-bearing atmospheres on the terrestrial planets. Approximately 30% of the known or probable terrestrial meteorite impact craters occur at least partially in carbonate rocks [Grieve and Robertson, 1979]. Impact-induced devolatilization of hydrous and carbonate minerals appears to play a role in the evolution of terrestrial planetary atmospheres [Lange and Ahrens, 1983, and unpublished manuscript, 1985].

Calcite phase transitions under static and dynamic loading have been the subject of many studies. Static compression studies indicate that two metastable polymorphs of calcite ($CaCO_3$), exist at pressures above that of the calcite-aragonite transition [Bridgman, 1939; Jamieson, 1957]. The single-crystal calcite Hugoniot shows density discontinuities at pressures of between 1.8 to 2.4 GPa, at about 3 GPa, at about 4.5 GPa, and at about 9.5 GPa, corresponding to the Hugoniot elastic limit (HEL) and the calcite I-II, II-III, and III-VI (see below) transitions, respectively [Ahrens and Gregson, 1964]. Analogous transitions occur in shocked limestone (polycrystalline calcite), although at somewhat lower pressures [Ahrens and Gregson, 1964; Grady et al., 1978; Grady, 1979]. The aragonite Hugoniot also displays evidence of several transitions [Vizgirda and Ahrens, 1982] which are probably unrelated to calcite II and III since aragonite is denser than these phases. Above about 10 GPa the single-crystal calcite [Ahrens and Gregson, 1964], polycrystalline calcite [Adadurov et al., 1961; Kalashnikov et al., 1973; van Thiel et al., 1977], and single-crystal aragonite [Vizgirda and Ahrens, 1982] Hugoniots are very similar, suggesting transformation to a similar high-pressure polymorph above that pressure. In the remainder of the text we refer to this stable high-pressure polymorph as calcite VI. Calcite IV and V are low-pressure, high-temperature forms of $CaCO_3$ [Carlson, 1983].

Release isentropes for polycrystalline calcite rocks shocked to pressures up to about 4 GPa have been determined using laser interferometry [Schuler and Grady, 1977; Grady et al., 1978; Grady, 1983] and electromagnetic particle velocity gauges [Murri et al., 1975; Larson and Anderson, 1979]. Murri et al. [1975] employed electromagnetic particle velocity gauges to determine release paths for selected carbonate rocks (porosity 0 and 15%) shocked to between 10 and 30 GPa. In this pressure range the initial release paths lie at greater densities than the Hugoniot. Release paths for single-crystal aragonite shocked to pressures up to 40 GPa have been determined using buffer and inclined mirror techniques [Vizgirda and Ahrens, 1982]. For shock pressures up to about 13 GPa the release paths are steep, and maximum postshock densities are greater than the initial densities. For shock pressures between about 13 and 40 GPa the release paths generally lie close to the Hugoniot, and maximum postshock densities are less than or equal to the initial density.

Incipient devolatilization (i.e., decomposition to CaO plus CO_2) of shock-loaded calcite has been reported for shock pressures as low as 10 GPa, with significant devolatilization (greater than 50%) occurring after shock compression to 20 GPa [Lange and Ahrens, 1983, and unpublished manuscript, 1985]. However, other studies suggest that incipient devolatilization occurs only at pressures of 18 GPa or higher, with only modest amounts of devolatilization (5-10%) at pressures of 50-60 GPa [Boslough et al., 1982; Kotra et al., 1983]. Theoretical calculations of postshock energy content assuming that the release path is identical to the Hugoniot require a shock pressure of 45 GPa for incipient devolatilization [Kieffer and Simonds, 1980] and consideration of postshock entropy content assuming isentropic release [Zel'dovich and Raizer, 1967; Ahrens and O'Keefe, 1972] indicates shock pressures of at least 33 GPa for incipient devolatilization [Vizgirda and Ahrens, 1982]. However, these previous experiments and calculations have failed to consider the effect of the

Paper number 4B5363.
0148-0227/86/004B-536$05.00

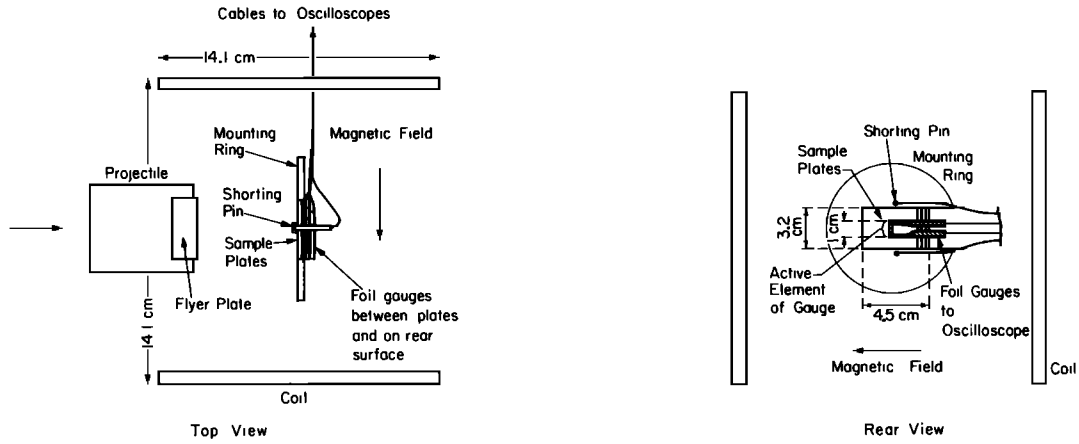

Fig. 1. Schematic diagram of particle velocity gauge experiment. Top view, active element of foil gauge is oriented in and out of plane of page. Gauges are epoxied between plates of Solenhofen limestone, and their electrical leads each go to an oscilloscope. Impact-induced velocity of gauge generates a voltage which is proportional to the magnetic field (generated by the Helmholtz coils). Pin signal triggers oscilloscopes.

ambient partial pressure of the volatile species on the equilibrium of the devolatilization reaction. The law of mass action indicates that low volatile partial pressures result in lower equilibrium temperatures for devolatilization reactions, which in turn lead to increased devolatilization for a given shock pressure.

Localization of thermal energy may also play a role in impact-induced devolatilization. A shock temperature measurement at 40 GPa on single-crystal calcite yields a color temperature of 3700 K, which is over twice the Hugoniot temperature calculated from continuum thermodynamic models, with an emissivity of 0.0025 [Kondo and Ahrens, 1983]. This result has been interpreted as indicating the presence of a large number of closely spaced high-temperature shear band regions immediately behind the shock front, in support of the shear instability models of Grady [1977, 1980] and Horie [1980]. These zones of intense heating would cause devolatilization to begin at much lower pressures than those calculated on the basis of continuum models.

We have determined the release paths for a slightly porous polycrystalline carbonate (Solenhofen limestone, $\rho_o = 2.58$ g/cm^3) shocked to pressures between 12 and 24 GPa and for a very porous calcite (Dover chalk, $\rho_o = 1.40$ g/cm^3) shocked to between 5 and 11 GPa pressure, using the electromagnetic particle velocity gauge technique. Release paths have not been previously determined for these materials shocked to these pressures. The sound velocity data obtained for the shocked state provide constraints on the mechanical strength properties under shock compression. We find that in the limestone a partial loss of shear strength occurs at shock pressures greater than about 20 GPa. This result is consistent with the concept of extensive formation of shear bands occurring in this pressure range but is not correlated with solid-solid phase transitions. The release path data are then used to evaluate a model for the postshock internal energy increase. The energy and entropy models are then employed in model equilibrium chemical calculations that demonstrate the effects of ambient P_{CO_2} on impact-induced devolitilization of calcite.

Experimental Technique

The particle velocity gauge technique used in these experiments is described elsewhere in detail [Boslough, 1983] and shown schematically in Figure 1. The targets consisted of four 1.5-mm-thick plates of Solenhofen limestone with 12.5-μm-thick copper, polyamide-backed (Kapton, 12.5 μm) particle velocity gauges epoxied between each plate and onto the free surface. The faces of the assembled target were parallel to within 25 μm. Archimedean and bulk densities were determined individually for each plate. The chalk target assemblies are shown in Figure 2. In the chalk assemblies the gauges were stretched across each plate and epoxied only on a 3-mm-wide strip along the plate edge. Because the chalk is relatively weak, each target assembly consisted of only three 2- to 2.5-mm-thick plates. Additional clamping was provided by a circular clamp ring on the front and clamping strips on the rear of the mounting ring.

The target was mounted at the center of a set of Helmholtz coils so that the active element of each gauge, the incident projectile velocity, and the magnetic field generated by the coils were mutually perpendicular. Upon impact a voltage is induced across the active element of the gauge which is proportional to the effective gauge (active element) length L, the magnetic induction B, and the particle velocity u_p,

$$V(t) = B\,L\,u_p(t) \quad (1)$$

where t is the time after impact. V(t) is in units of volts when B is in gauss, L is in centimeters, and u_p is in centim-

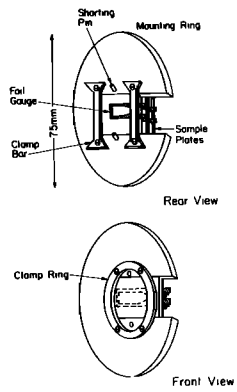

Fig. 2. Chalk (porous calcite) target assembly. Electrical leads from gauges and pins are omitted for clarity.

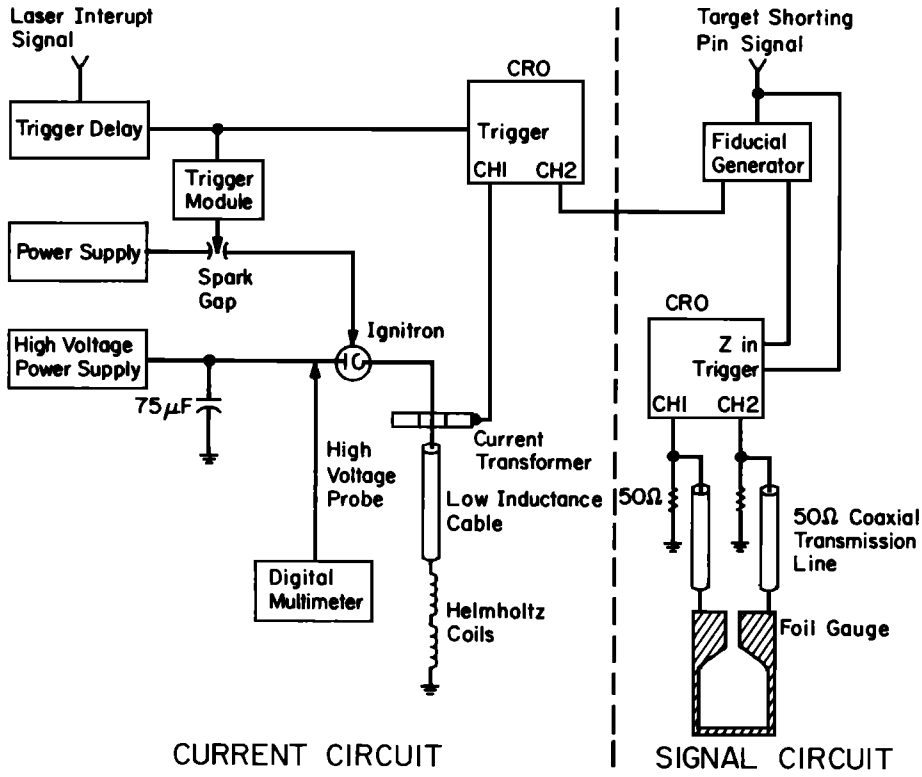

Fig. 3. Schematic diagram of current-generating and signal-measuring circuits. Only one of four signal circuits is shown.

eters per second. In these experiments, B was approximately 1.8 kG, and L was approximately 0.95 cm. The gauge voltages were recorded by a series of four Tektronix oscilloscopes using the circuits sketched in Figure 3.

The shots were performed on the 40-mm propellant gun at the California Institute of Technology [Ahrens et al., 1971]. The impact tank pressure was between 50 and 160 μm Hg. Fused quartz and polycrystalline alumina flyer plates between 6 and 18 mm thick were employed. The projectile velocity was measured by determining the flight distance of the projectile during the known time interval between two flash X ray photographs of the projectile.

Typical experimental results are shown in Figure 4, which shows particle velocity versus time after impact obtained from digitized oscilloscope records. The shock wave generated by the impact reaches each of the gauges in sequence (gauge 1 is nearest the impacted surface, gauge 4 is on the rear, or free, surface) accelerating it to the particle velocity of the Hugoniot state. Gauge 4 is accelerated immediately to the free surface velocity. Gauge 3 and then gauge 2 are later accelerated to higher particle velocities by the rarefaction wave propagating back into the sample from the free surface. Gauge 2 is disrupted by rarefactions originating at the edges of the target before reaching the final free surface velocity. Gauge 1 is intercepted by the forward traveling rarefaction originating at the upstream side of the flyer plate and is therefore accelerated to lower particle velocities. These relationships are shown more clearly in a schematic position-time (x-t) plot, shown in Figure 5.

The time interval between the shock arrival at each gauge was used to determine the shock wave velocity. This was combined with the projectile velocity and the known flyer material Hugoniot [Marsh, 1980] in an impedance match solution [McQueen et al., 1970] to yield the Hugoniot state. The Hugoniot particle velocity obtained in this way provided the reference point for the gauge voltage versus particle velocity calibration.

The stress and density along the release path are given by equations for conservation of mass and linear momentum [Cowperthwaite and Williams, 1971]:

$$\left(\partial\rho/\partial u_p\right)_h = \frac{\rho^2}{\rho_o} C_u \tag{2}$$

$$\left(\partial\sigma/\partial u_p\right)_h = \rho_o C_\sigma \tag{3}$$

where ρ is the density, ρ_o is initial density, u_p is particle velocity, h is the Lagrangian space coordinate, and

$$C_u = (\partial h/\partial t)_u \tag{4a}$$

$$C_\sigma = (\partial h/\partial t)_\sigma \tag{4b}$$

where t is time. C_u is the velocity of propagation of a wave with particle velocity u_p, and C_σ is the velocity of propagation of a wave of stress σ. The release waves are nonsteady simple waves [Courant and Friedrichs, 1948; Petersen et al., 1970]. Therefore C_u and C_σ are equal but depend on u_p. The digitized particle-velocity-as-a-function-of-time records were used to compute C_u and then equations (2) and (3) were integrated numerically to obtain the stress-density path of the release. The Lagrangian sound speed, C_u, is obtained using the finite difference approximation,

$$C_u \approx \frac{\Delta h}{\Delta t} \tag{5}$$

where Δh is the initial distance between gauges and Δt is the transit time for a disturbance with a particle velocity u_p. Eulerian sound speeds are equal to

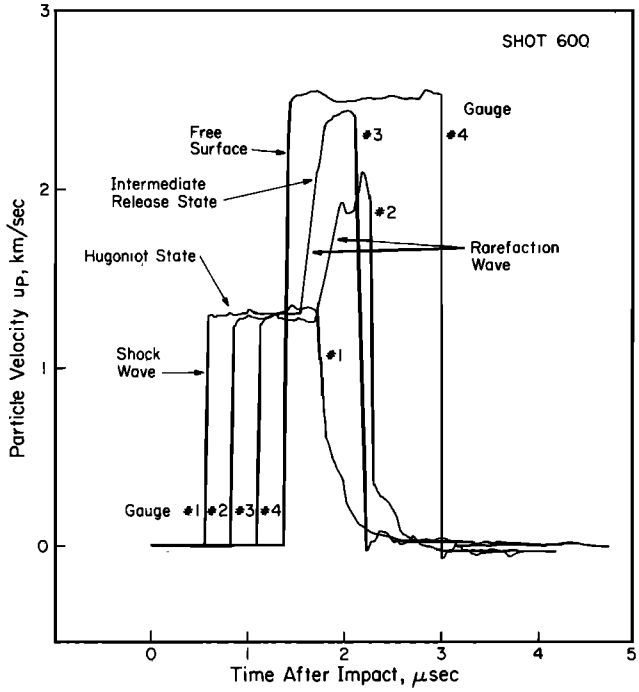

Fig. 4. Particle velocity versus time after impact for shot 600 obtained from digitized voltage versus time oscilloscope records. Gauge 1 is nearest to impacted surface, gauge 4 is at free surface. Shock velocity was 5.741 km/s, Hugoniot particle velocity was 1.319 km/s, and shock pressure was 19.75 GPa.

$$C_E = \frac{\rho_o}{\rho} C_u \qquad (6)$$

The Eulerian sound speed corresponds to the sound speed relative to the laboratory reference frame.

Results

The experimental results for the shocked states of the Solenhofen limestone and the Dover chalk are summarized in Table 1. Figures 6 and 7 are shock velocity-particle velocity (U_s–u_p) and pressure-density (P-ρ) plots of the data, respectively. The experimental data for shot 599 (Dover chalk) appear to be erroneous. The results are listed in Table 1 but are not plotted. No release path data were obtained from shot 601.

In two of the shots, shots 596 and 602 (Hugoniot pressures 13.10 and 11.96 GPa, respectively), multiple wave structure was observed (Figure 8). Transitions occurring between 0.36 and 0.45 GPa and between 2.5 and 3.7 GPa were identified. Multiple wave structure has been observed in previous shock wave experiments on carbonates and is caused by dynamic yielding and at least three additional phase changes that calcite undergoes at low pressures [Ahrens and Gregson, 1964; Grady et al., 1978]. However, in the experiments reported here the shock and particle velocities of the intermediate states are poorly constrained and are not completely consistent. These less reliable data are shown in parentheses in Table 1.

The velocity of 5.7 ± 0.3 km/s for the first wave of shot 602 (Table 1) is comparable to the ultrasonically determined longitudinal wave velocity of Solenhofen limestone, 5.84-5.97 km/s [Peselnick, 1962; Hughes and Cross, 1951], indicating that this transition represents the Hugoniot elastic limit (HEL). Ahrens and Gregson [1964] report elastic precursor velocities of 5.3-5.7 km/s and a

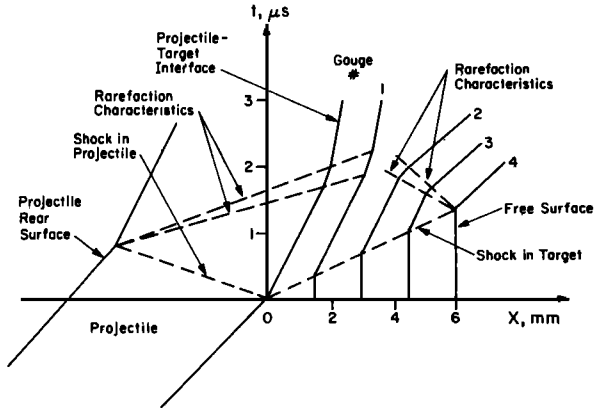

Fig. 5. Position-time (x-t) diagram of a particle velocity experiment. Projectile approaches from left and impacts stationary target at x=0, t=0. The diagram shows the (undesirable) case in which gauge 1 is intercepted by the rarefaction propagating forward from the projectile rear surface before arrival of rarefaction from rear surface.

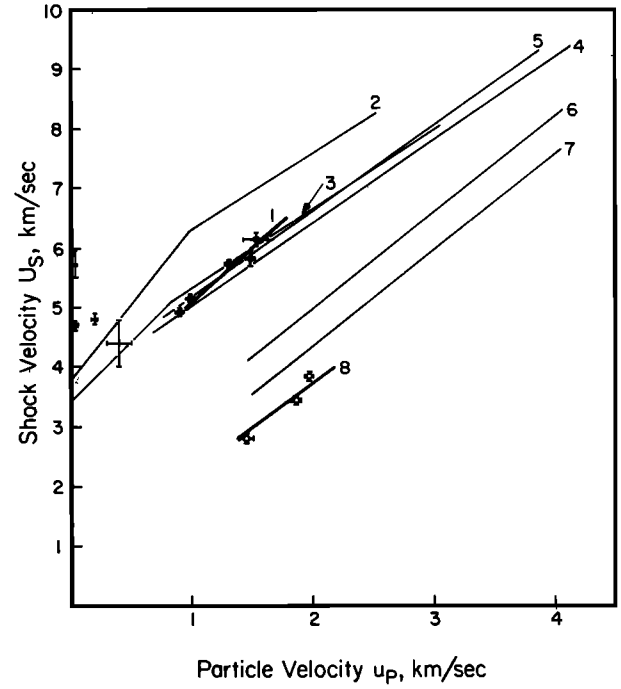

Fig. 6. Shock wave velocity U_s versus particle velocity u_p data for experiments reported here and comparison with previous results. Filled symbols show present data for the Solenhofen limestone, open symbols show data for Dover chalk. Crosses with no symbol represent intermediate states. Lines represent fits of form $U_s = C_o + s\,u_p$. Parameters for fits are listed in Table 2. Curves are labeled as follows: 1, Solenhofen limestone, this study, ρ_o = 2.594; 2, single crystal aragonite [Vizgirda and Ahrens, 1982], ρ_o = 2.93; 3, polycrystalline calcite [Adadurov et al., 1961], ρ_o = 2.703; 4, Solenhofen limestone [van Thiel et al., 1977], ρ_o = 2.585; 5, polycrystalline calcite [Kalashnikov et al., 1973], ρ_o = 2.665; 6, polycrystalline calcite [Kalashnikov et al., 1973], ρ_o = 2.02; 7, polycrystalline calcite [Kalashnikov et al., 1973], ρ_o = 1.705; 8, Dover chalk, this study, ρ_o = 1.40. Units of density are grams per cubic centimeter.

TABLE 1. Summary of Intermediate, State, Hugoniot State, and Release Path Release Transition Data

Shot	Projectile Material	Projectile Velocity V_p, km/s	Initial Density ρ_o, g/cm^3	Shock States[a] Shock Velocity U_s, km/s	Particle Velocity u_p, km/s	Pressure P, GPa	Density ρ, g/cm^3	Release Path Phase Transitions Particle Velocity u_{p1}, km/s	Pressure P_1, GPa	Density ρ_1, g/cm^3
				Solenhofen Limestone						
590	Al_2O_3	2.209 ±0.017	2.591 ±0.010	5.819 ±0.150	1.487 ±.018	22.41 ±0.44	3.480 ±0.042	2.44 ±0.10	6.48 ±1.27	2.90 ±0.08
596	fused quartz	2.158 ±0.020	2.584 ±0.009	(4.60) ±0.08	(0.030) ±0.010	(0.36) ±0.12	(2.601) ±0.021	1.26 ±0.03	8.20 ±0.60	3.11 ±0.02
				(4.415) ±0.435	(0.40) ±0.10	(4.58) ±1.05	(2.841) ±0.079			
				5.081 ±0.080	0.997 ±0.015	13.10 ±0.16	3.215 ±0.021			
598	Al_2O_3	2.310 ±0.150	2.584 ±0.010	6.073 ±0.120	1.538 ±0.110	24.14 ±1.67	3.461 ±0.085	2.65 ±0.06	3.21 ±0.80	2.87 ±0.04
600	Al_2O_3	1.965 ±0.005	2.608 ±0.002	5.741 ±0.008	1.319 ±0.004	19.75 ±0.06	3.386 ±0.004	2.11 ±0.04	4.97 ±0.51	2.95 ±0.03
602	fused quartz	1.992 ±0.010	2.604 ±0.005	(5.706) ±0.300	(0.030) ±0.010	(0.45) ±0.15	(2.618) ±0.021	1.34 ±0.04	5.97 ±0.47	3.00 ±0.02
				(4.774) ±0.090	(0.200) ±0.020	(2.56) ±0.30	(2.715) ±0.025			
				4.903 ±0.050	0.936 ±0.008	11.96 ±0.09	3.219 ±0.013			
				Dover Chalk						
599	Al_2O_3	2.078 ±0.015	1.434 ±0.030	3.750 ±0.100	1.745 ±0.018	9.39 ±0.26	2.683 ±0.085			
601	Al_2O_3	2.331 ±0.020	1.434 ±0.030	3.845 ±0.050	1.959 ±0.020	10.80 ±0.22	2.924 ±0.066			
620	Al_2O_3	1.619 ±0.019	1.365 ±0.024	2.933 ±0.047	1.414 ±0.180	5.66 ±0.13	2.635 ±0.064			
622	Al_2O_3	2.235 ±0.022	1.365 ±0.024	3.652 ±0.127	1.900 ±0.023	9.47 ±0.32	2.846 ±0.131			

[a] Highest-pressure state is final shock state. All others are intermediate states.
Values in parentheses are less reliable data.

HEL of 1.0-1.5 GPa for carbonate-bearing rocks. Grady et al. [1978] report a break in the Solenhofen limestone loading wave profile at 0.6 GPa and conclude that the calcite I-II phase transition occurs at this pressure, coincident with the onset of dynamic yielding. Our data are not of sufficient resolution in this pressure range to resolve this question. Comparison with the results of Grady et al. [1978] suggests that the transition at 2.5-3.7 GPa corresponds to the calcite II-III transition. In the higher shock pressure shots these transitions are apparently overdriven, in agreement with previous shock experimental results [Ahrens and Gregson, 1964]. No precursory waves were observed in the shots on Dover chalk.

Figure 6 shows the U_s–u_p data determined in this study compared to trends observed in various calcium carbonate-bearing rocks and minerals by previous investigators. For Solenhofen limestone the values of U_s and u_p lie within the range of values previously determined by other investigators, but the slope of the line defined by the data is greater. The data in the range of 12 to 24 GPa can be fit by an equation of the form

$$U_s = C_o + s\,u_p \qquad (7)$$

where C_o and s are constants, with $C_o = 3.269$ km/s and $s = 1.796$ ($r^2 = 0.97$). Previously determined values of C_o and s range from 3.62 to 3.99 km/s and 1.32 to 1.61, respectively, and are summarized in Table 2. The U_s–u_p data for Dover chalk, $\rho_o = 1.40$ g/cm^3, can be fit with $C_o = 0.667$ and $s = 1.598$ ($r^2 = 0.989$). This line is consistent with the trend formed by the porous calcite results of Kalashnikov et al. [1973].

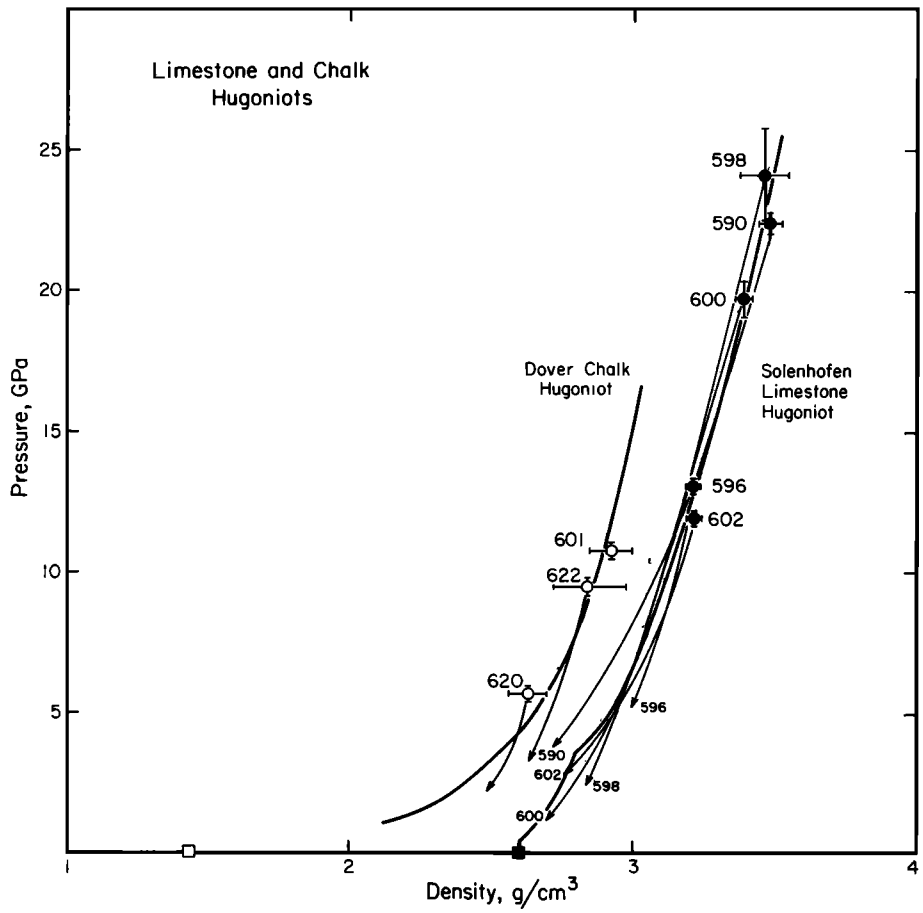

Fig. 7. Hugoniot states and release paths for Solenhofen limestone and Dover chalk. Solid symbols are for Solenhofen limestone; open symbols are for Dover chalk, squares represent initial densities. Heavy solid lines are fits to data (Table 2).

As shown in Figures 4 and 8, the slopes of the particle velocity records of all the Solenhofen limestone shots exhibit a discontinuity during release. The pressures and densities at which the discontinuity occurs for each shot are listed in Table 1. The data are somewhat scattered but the transition occurs at about 5.5±2.5 GPa, and no trend with peak stress level is apparent. Previous observations of a phase transition upon release in calcite shocked up to 5 GPa have been attributed to the calcite III-II transition [Grady et al., 1978]. Rarefaction shocks have been observed in calcite shocked to between 18 and 31 GPa [Murri et al, 1975; Grady and Moody, 1985]. Rarefaction shocks are not evident in the particle velocity records reported here. However, the pressures behind the rarefaction shocks reported by the previous investigators correspond roughly to the stress levels at which we observe the particle velocity slope discontinuities. We thus interpret the discontinuities as indicating a high-pressure (calcite VI) to low-pressure (unspecified) polymorphic transition during the release.

The initial release paths for Solenhofen limestone plotted in Figure 7 lie near the Hugoniot, but at slightly higher densities, for all shock pressures studied. The particle velocity records do not give complete information down to zero pressure due to disruption of the foil gauges by rarefactions propagating inward from the sample edges. Extrapolation to zero-pressure yields complete release densities between 2.59 and 2.81 g/cm^3. In contrast to the behavior for Solenhofen limestone reported here, previously reported release paths for single crystal aragonite vary significantly

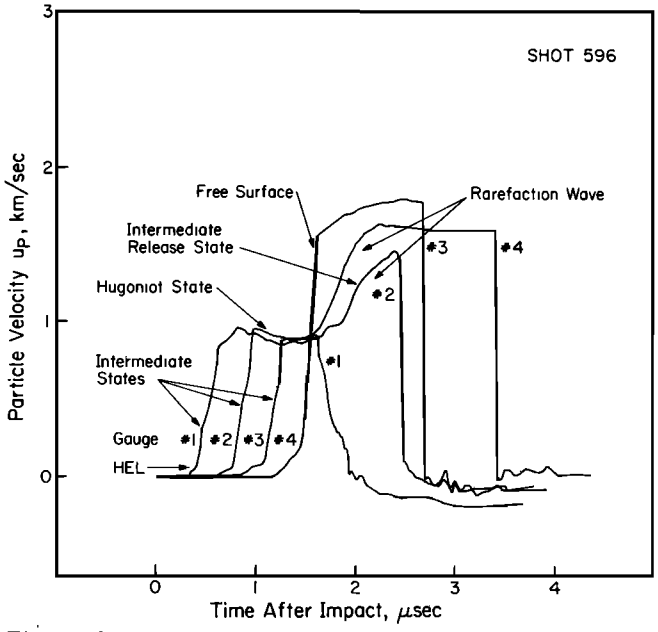

Fig. 8. Particle velocity versus time after impact for shot 596 (Solenhofen limestone, 13.1 GPa), showing multiple shock fronts on leading edge of record (including HEL) and indicating presence of an intermediate release state during unloading.

TABLE 2. Summary of Polycrystalline Calcite Hugoniot Data

Material	Reference	ρ_o, g/cm^3	C_o, km/s	s	Pressure Range, GPa
Solenhofen limestone	this work	2.594	3.269	1.796	12-24
Dover chalk	this work	1.40	0.67	1.60	5-11
Polycrystalline calcite	Adadurov et al., 1961	2.703	3.40	2.00	5-13
			3.99	1.32	13-51
Polycrystalline calcite	Kalashnikov et al., 1973	2.665	3.70	1.44	10-94
		2.020	1.74	1.61	13-71
		1.705	1.15	1.60	10-59
Solenhofen limestone	van Thiel et al., 1977	2.585	3.62	1.39	8-90

with shock pressure. For shock pressures between about 10 and 15 GPa the aragonite release paths are very steep, with complete release densities (determined via inclined mirror experiments) equal to or greater than the initial density. For shock pressures greater than about 20 GPa, the release paths approximate the Hugoniot, with complete release densities equal to or less than the initial density [Vizgirda and Ahrens, 1982]. Release paths for Solenhofen limestone [Schuler and Grady, 1977] and other carbonate rocks [Grady et al., 1976; Grady, 1983] shocked to pressures up to about 5 GPa generally follow the Hugoniot, with extrapolated complete release densities approximately equal to the initial density.

The release paths for Dover chalk lie at higher densities than the Hugoniot. The extrapolated complete release densities lie between 2.44 and 2.55 g/cm^3. Eulerian sound speeds for the shocked states were calculated according to equations 5 and 6 and are plotted in Figure 9.

Discussion

Sound Speeds and Shear Strength

Properties of calcite VI, reached at about 10 GPa shock pressure, have been deduced by Vizgirda and Ahrens [1982] and are listed in Table 3. The zero-pressure bulk sound velocity

$$V_\phi = (K_{os}/\rho_o)^{1/2} \quad (8)$$

where K_{os} is the zero-pressure isentropic bulk modulus, is between about 5.00 and 5.54 km/s at 300 K. Assuming a Poisson's ratio σ of 0.25 we obtain a zero-pressure, 300 K compressional velocity V_p of between 6.46 and 7.15 km/s using the relationship

$$V_p = \left\{K_{os}/\rho \cdot [1+2\,(1-2\sigma)/(1+\sigma)]\right\}^{1/2} \quad (9)$$

We can compare the observed Hugoniot sound velocities with compressional wave velocities V_p along an isentrope for calcite VI using finite strain theory [Sammis et al., 1970] (see also Burdick and Anderson [1975]). Thus

$$V_p^2(\rho) = V_{p,o}^2\,(1-2\epsilon)\,[1-2\epsilon(3\,D_p - 1)] \quad (10)$$

$$V_s^2(\rho) = V_{s,o}^2\,(1-2\epsilon)[1-2\epsilon(3\,D_s - 1)] \quad (11)$$

and

$$P = -3K_{os}\,\epsilon\,(1-2\epsilon)^{5/2}\,(1+2\epsilon\,\xi). \quad (12)$$

The volumetric strain ϵ is

$$\epsilon = [\,1 - (\rho/\rho_o)^{2/3}\,]/2 \quad (13)$$

the finite strain parameter ξ is

$$\xi = 3\,[4 - (d\,K_{os}/dP)_s]/4 \quad (14)$$

$$D_p = K_{os}\,d\,ln\,V_p/d\,P \quad (15)$$

and

$$D_s = K_{os}\,d\,ln\,V_s/d\,P \quad (16)$$

No determinations of D_p and D_s for calcite VI exist. For many minerals, D_p lies in the range $1.0 \leq D_p \leq 1.6$, and D_s lies between $0.1 \leq D_s \leq 1.0$ [Anderson et al., 1968; Sammis et al., 1970]. This range of values was used in computing $V_p(\rho)$ and $V_s(\rho)$. The variation of bulk sound speed V_ϕ along an isentrope is given by

$$V_\phi^2(\rho) = V_p(\rho)^2 - 4\,V_s^2(\rho)/3 \quad (17)$$

The effect of temperature on sound velocity is small. The temperature on the Hugoniot T_H was calculated using the relation

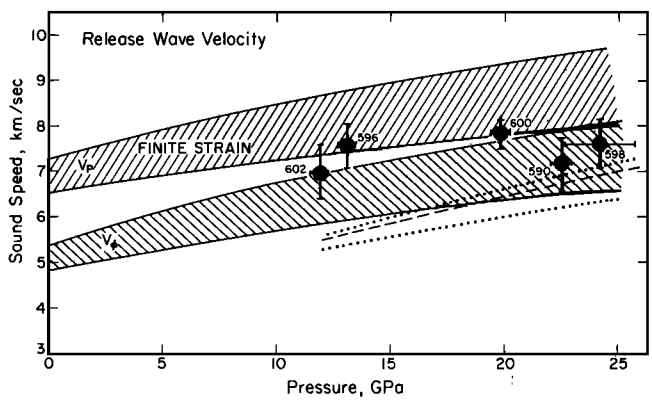

Fig. 9. Eulerian sound speeds, C_E, on the Hugoniot of shocked Solenhofen limestone. Ranges of compressional wave velocity V_p and bulk sound speed V_ϕ for calcite VI are computed using Eulerian finite strain theory (see text) and parameters listed in Table 3. Values plotted are for an isentrope originating at 750 K at zero pressure. Dashed line is V_ϕ along the Hugoniot of calcite VI calculated according to equation (19) using equation of state parameters determined in this work (Table 2) and Gruneisen parameter γ given in Table 3. Dotted lines show effect of a factor of 2 variation in γ.

TABLE 3. Properties of the Calcite Polymorphs

Property	Symbol (Units)	I	II	III	VI
STP density (300 K)	ρ_o (g/cm^3)	2.71[a]	2.71[a]	2.71[a]	3.0-3.1[b]
Isentropic bulk modulus	K_{os} (GPa)	71.1[a]	14.7[a]	51.7[a]	75-95[b]
dK/dP	K'	4.15[a]	4.62[a]	8.28[a]	4.1-3.5[b]
Transition energy	E_{tr} (J/g)[c]	0	-	-	200-20[b]
Transition entropy	S_{tr} (J/g K)[c]	0	-	-	-0.101
Gruneisen parameter	γ	1.5 (V/V_o)[d]	1.5 (V/V_o)[d]	1.5 (V/V_o)[d]	1.5 (V/V_o)[d]
Poisson's ratio	σ	0.25[d]	0.25[d]	0.25[d]	0.25[d]
K_{os}·d ln V_p/dP	D_p	2.13[e]	0.44[e]	1.55[e]	1.0-1.6[f]
K_{os}·d ln V_s/dP	D_s	2.13[e]	0.44[e]	1.55[e]	1.0-0.1[f]
d V_p/dT	(km/s K)	-3.3×10^{-4}[f]	-3.3×10^{-4}[f]	-3.3×10^{-4}[f]	-3.3×10^{-4}[f]
d V_s/dT	(km/s K)	-2.4×10^{-4}[f]	-2.4×10^{-4}[f]	-2.4×10^{-4}[f]	-2.4×10^{-4}[f]
Specific heat	C_v (J/g K)	1.25[g]	1.25[g]	1.25[g]	1.25[g]

[a] Singh and Kennedy [1974].
[b] Vizgirda and Ahrens [1982].
[c] Relative to calcite I at 298K, 1 bar
[d] Assumed.
[e] Peselnick and Wilson [1968] and Wang and Meltzer [1973].
[f] Anderson et al. [1968] and Sammis et al. [1970].
[g] Dulong-Petit value, $T \geq 650$ [Vizgirda and Ahrens, 1982]; at lower temperatures C_p of calcite given by Robie et al. [1978].

$$T_H = 298 \exp\left[-\int_{V_o'}^{V_H} \frac{\gamma}{V}\, dV\right] + \left[\frac{1}{2}(P_O + P_H)(V_O - V_H) + \int_{V_o'}^{V_H} (PdV)_s\right] / C_V \quad (18)$$

where γ is the Gruneisen parameter and C_V is the heat capacity at constant volume. V_O refers to the initial volume of the experimentally shocked material, whereas V_O' is the volume at standard temperature and pressure (STP) conditions of the high-pressure polymorph, calcite VI. The energy of transition E_{tr} does not enter into the temperature calculation because, in performing the calculation, the calcite I to VI transition occurs isothermally at STP. The first term on the right-hand side of equation (18) is the temperature increase between V_O' and V_H along the calcite VI adiabat, and the second term represents the temperature increase in going from the adiabat to the Hugoniot isochorically at V_H. The parameters used for the calculation of T_H are listed in Table 3. For the Dover chalk, the temperatures are sufficiently high that calculated Hugoniot temperatures are relatively insensitive to the specific isentrope employed in the calculation. Assuming a value of $(d V_p/dT)_p$ of -3.3 x 10^{-4} km/s K (values tabulated by Anderson et al. [1968] range from about -1.5 x 10^{-4} to -5.2 x 10^{-4} km/s K), an increase in the initial temperature of 450 K results in a V_p decrease of 0.15 km/s. $(dV_s/dT)_p$ is estimated to be about -2.4 x 10^{-4} km/s K [Anderson et al., 1968].

The range of values of V_p and V_ϕ along a 750 K isentrope calculated using the parameters listed in Table 3 is shown in Figure 9. Although the calculated bulk and compressional sound speeds are poorly constrained, the data indicate that the measured initial release wave speed is equal to that of the compressional wave velocity for shock pressures up to about 20 GPa. In other words, calcite VI retains its shear strength in the shocked state up to this pressure. At the highest pressures attained, 22-24 GPa, a loss of strength in the shocked state may occur.

The bulk sound speed V_ϕ at the Hugoniot may also be calculated from the shock wave equation of state (equation (7)) and a model for the Gruneisen parameter γ, using the relationship

$$V_\phi = V_H\left\{\frac{dP}{dV}\Big|_H\left[(V_o - V_H)\frac{\gamma}{2V_H} - 1\right] + P_H\gamma/2V_H\right\}^{1/2} \quad (19)$$

[McQueen et al., 1967] where V_o is the initial sample volume, V_H is the Hugoniot volume, and $dP/dV|_H$ is the slope of the Hugoniot. We use the relationship $\gamma = \gamma_o(\rho_o/\rho)^n$ where $\gamma_o = 1.5$ and $n = 1.0$ [Vizgirda and Ahrens, 1982] (Table 3). This curve is plotted as a dashed line in Figure 9 and supports the conclusion that at least a partial loss of shear strength occurs at a pressure of 22-24 GPa. A variation in γ of a factor of 2 from the above value does not change the conclusion (dotted lines in Figure 9).

The Eulerian sound speeds along the release paths of the shocked Dover chalk are plotted in Figure 10. At the relatively low shock pressures and high continuum temperatures reached in these experiments it is unlikely that the starting material transformed to calcite VI. However, it is not known which of the three calcite low-pressure

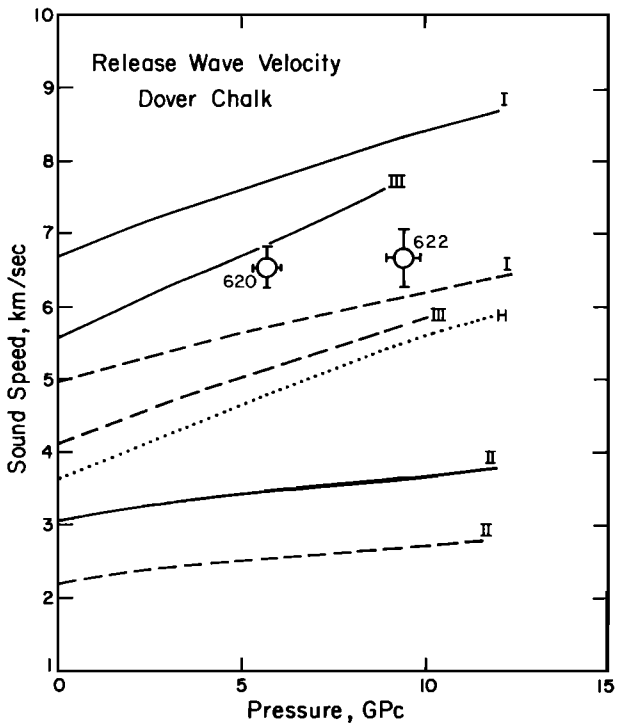

Fig. 10. Eulerian sound speeds C_E on Hugoniot of Dover chalk. Solid and dashed lines represent compressional wave velocities and bulk sound velocities, respectively, of calcite polymorphs along isentropes centered at 750 K and ambient pressure, calculated using the parameters in Table 3. Roman numerals refer to the assumed calcite polymorph. Dotted line labeled H represents bulk sound speed along low-pressure (5-13 GPa) polycrystalline calcite Hugoniot of Adadurov et al. [1961] (Table 2) using equation (19).

polymorphs exists in the shocked state. We have therefore plotted the bulk and compressional wave velocities for calcite I, II, and III using, for comparison, the data of Singh and Kennedy [1974], assuming that Poisson's ratio σ = 0.25 [Anderson et al., 1968; Grady et al., 1978]. Also plotted is the bulk sound speed in the shocked state calculated using the low pressure (5-13 GPa) polycrystalline calcite Hugoniot of Adadurov et al. [1961] and equation (19). The data for shots 620 and 622 plot between the bulk and compressional wave velocities for calcite I and III, but the result for shot 622 (P_H = 9.47 GPa) lies nearer the bulk sound speed of calcite I and III.

An alternative approach is to assume that the measured initial release wave velocities correspond to the bulk sound speeds, then to calculate γ using equation (19). However, the values of γ calculated this way are less than zero for all the shots in both materials, save one (shot 590, Solenhofen limestone, 22.4 GPa, yields γ = 0.23). These nonphysical results are a further indication that the measured release wave velocities are compressional wave velocities and that Solenhofen limestone and Dover chalk retain their shear strength in the Hugoniot state. The intermediate value of γ at 22.4 GPa for the Solenhofen limestone is an indication of at least a partial loss of shear strength.

Retention of shear strength in the shocked state has been documented for several materials, for example, Al_2O_3 shocked to 40 GPa [Bless and Ahrens, 1976], MgO to 12 GPa [Grady, 1977], and anorthosite to 10 GPa [Boslough and Ahrens, 1985]. Loss of shear strength in materials shocked to pressures lower than those required for bulk melting of the sample has been reported for quartz shocked to 15-40 GPa [Grady et al., 1975] and for calcite rocks to about 5 GPa [Grady et al., 1978]. Both quartz and calcite undergo solid-solid phase transitions throughout these pressure ranges. In these materials, the loss of shear strength is apparently caused by the occurrence of molten "shear bands" caused by localization of thermal energy under shock compression. The rates of the solid-solid phase transitions are enhanced by the existence of, and high temperatures in, the molten regions [Grady et al., 1975; Grady, 1980]. The reduction of shear strength of Solenhofen limestone at 22-24 GPa indicates that extensive shear band formation can occur in the absence of bulk solid-solid phase transformation. The measured color temperature (shear band temperature) of 2455 K at 22 GPa (D. Schmitt, personal communication, 1984) supports this conclusion. Thus the occurrence of solid-solid phase transitions under shock implies thermal energy localization (shear bands), but the existence of shear bands (as indicated by loss of shear strength and by very high color temperatures) is not an indication of, nor is it dependent on, solid-solid transitions.

Impact–Induced Devolatilization

Recent shock recovery experiments on single crystal calcite have given differing results for the extent of impact-induced devolatilization as a function of shock pressures. The process under discussion can be described by the reaction

$$CaCO_{3(I)} \rightarrow \text{impact, release} \rightarrow CaO_{(s)} + CO_{2\,(gas)} \quad (20)$$

The gas recovery experiments of Boslough et al. [1982] indicated that incipient devolatilization (0.03-0.3 % devolatilization) occurred at a shock pressure of 18 GPa. Solid recovery experiments by Lange and Ahrens [1983] resulted in roughly 30-40 % devolatilization at 20 GPa, with incipient devolatilization occurring at less than 10 GPa. Solid recovery experiments by Kotra et al. [1983] yielded very little devolatilization, only 5-10 % devolatilization took place at shock pressures up to 50-60 GPa. In the following sections we compare these experimentally determined values of the fraction of CO_2 volatilized with calculations based on postshock energy and entropy content.

The energy imparted to a material upon shock compression E_H relative to the energy of the initial state E_O is

$$E_H - E_o = \frac{1}{2}(P_H + P_o)(V_o - V_H) + E_{tr} \quad (21)$$

where E_{tr} is the energy of transition from the low pressure to the high-pressure polymorph (if such a transition occurs). The energy released upon relaxation to zero pressure E_{rel} is

$$E_{rel} - E_H = -\int_{V_H}^{V_\infty} P_s dV + E'_{tr} \quad (22)$$

where V_∞ is the complete release volume, the integral is taken along the appropriate (see below) isentrope, and E'_{tr} is the energy of phase changes that occur during release (see below). The total post-shock energy E_p (relative to the initial energy content E_o) is the sum

$$E_p - E_o = (E_H - E_o) + (E_{rel} - E_H) \quad (23)$$

The release paths for the shots reported here can be integrated directly (with extrapolation to zero pressure) to yield the first term on the right-hand side of equation (22). In addition, the particle velocity records indicate that a phase transition occurs at some pressure greater than zero upon release, although the precise nature of the phase change is uncertain (see results section). For simplicity, we assume that the transition involved is from the calcite VI polymorph back to calcite I. Thus $E_{tr} = -E'_{tr}$, and

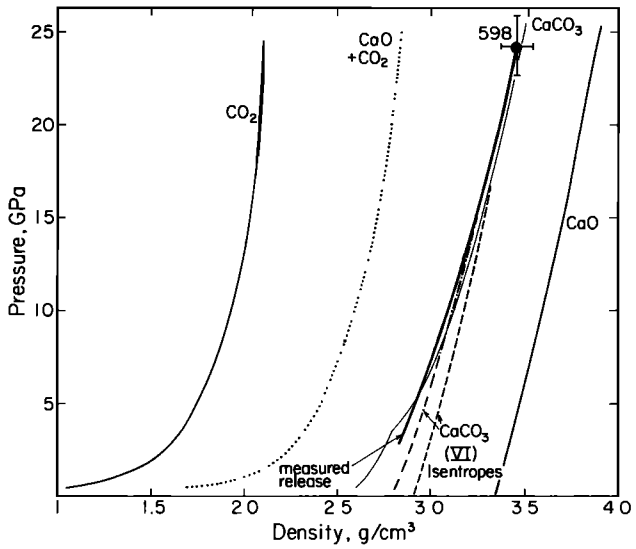

Fig. 11. Measured release path for Solenhofen limestone shocked to 24 GPa (shot 598), heavy line, relative to isentropic release of calcite VI; dashed line, K = 95 GPa, K' = 3.5; dash-dot line, K = 75 GPa, K' 4.1 GPa. Lines "CaO" and "$CaCO_3$" are Hugoniots (CaO Hugoniot, B1 phase [Jeanloz and Ahrens, 1980]). Line "CO_2" is the density of CO_2 at the P and T of the calcite VI isentrope, calculated by extrapolation of the equation of state of Kerrick and Jacobs [1981]. The dotted line "CaO + CO_2" is the density of an equimolar mixture of CaO and CO_2.

$$E_p - E_o = \frac{1}{2}(P_H + P_o)(V_o - V_H) - \int_{V_H}^{V_\infty} (PdV)_{\text{release path}} \quad (24)$$

Figure 11 shows, as an example, the measured release path from 24 GPa (shot 598) and isentropes of calcite VI (Table 3) centered on the Hugoniot. The data lie very close to the calculated isentropes, indicating that to a reasonable degree of accuracy, the integral along the actual release path in equation (24) may be approximated by the integral along the calcite VI isentrope. Thus, for purposes of calculation and generalization, the postshock energy increase is given by

$$E_p - E_o = \frac{1}{2}(P_H + P_o)(V_o - V_H) - \int_{V_H}^{V_\infty} (P_s d\,V)_{\text{calcite VI}} \quad (25)$$

For the Dover chalk, anomalies in the Hugoniot or the release data are not observed; therefore we assume that transformation to calcite VI does not occur in the pressure range studied. Thus, in equation (25) the integration is carried out using the calcite I and II isentropes as limiting cases.

Figure 11 also shows the density of an equimolar mixture of CaO and CO_2 at the temperatures and pressures of the calcite VI isentrope centered at the 24 GPa data point. The density of CaO is approximated by the CaO (B1 phase) Hugoniot [Jeanloz and Ahrens, 1980]. The CO_2 density was estimated for each PT point of the isentrope by extrapolation of the equation of state proposed by Kerrick and Jacobs [1981]. Use of the CO_2 equation of state of Bottinga and Richet [1981] yields similar values. Extrapolation of these equations of state to the temperatures and pressures considered here is, of course, extremely speculative because the data on which they are based extend up to only 1273 K and 0.8 GPa. The calculated CaO + CO_2 curve indicates that if complete devolatilization occurred during the portion of the release measured, a much lower density release curve would be expected. However, within the error limits of the Hugoniot data and the release path, up to about 15% devolatilization at the lowest pressure point on the release path (~2.5 GPa) cannot be ruled out. For definitive determination of the exact point during (or immediately subsequent to) release at which devolatilization commences, more precise determinations of the release path must be made down to lower pressures.

Figure 12 shows the postshock energy gain versus pressure for the experimental data (using equation (24)) and for the model calculation (equation (25)). The agreement between the two indicates that the model used and the parameters employed (Table 3) provide a self-consistent representation of the energy changes involved in shock compression and release of calcite. We can now compare the postshock energy content of the calcite with the energy required for devolatilization E_{IV}.

The energy required for incipient decarbonation (volatilization) E_{IV} can be calculated using the data of Robie et al. [1978]. It is important to bear in mind that the equilibrium of the reaction

$$CaCO_{3\,(\text{calcite})} \rightleftarrows CaO_{(\text{solid})} + CO_{2\,(\text{gas})} \quad (26)$$

is strongly influenced by the ambient pressure of CO_2, P_{CO_2}. Thus for pure solid calcite and pure solid CaO, the Gibbs free energy of reaction (26) ΔG_{rx} is

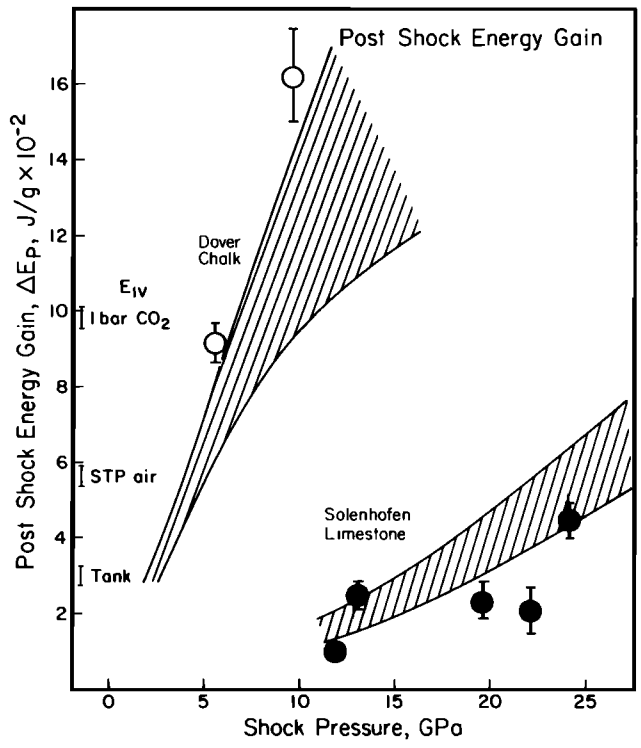

Fig. 12. Postshock energy increase ΔE_p as a function of shock pressure. Data points show ΔE_p calculated from the experimental release paths, using equation (24). Hatched regions represent values of ΔE_p calculated using calcite VI parameters (Table 3) for Solenhofen limestone and calcite I and II parameters for Dover chalk, using equation (25). The Hugoniot pressure of the porous material was calculated using equation (31). Also shown is energy of incipient vaporization E_{IV} calculated for several values of P_{CO_2}. "STP air" refers to P_{CO_2} in dry air, 3.3×10^{-4} bars; "Tank" refers to P_{CO_2} in impact tank under shot conditions, about 4.3×10^{-8} bars.

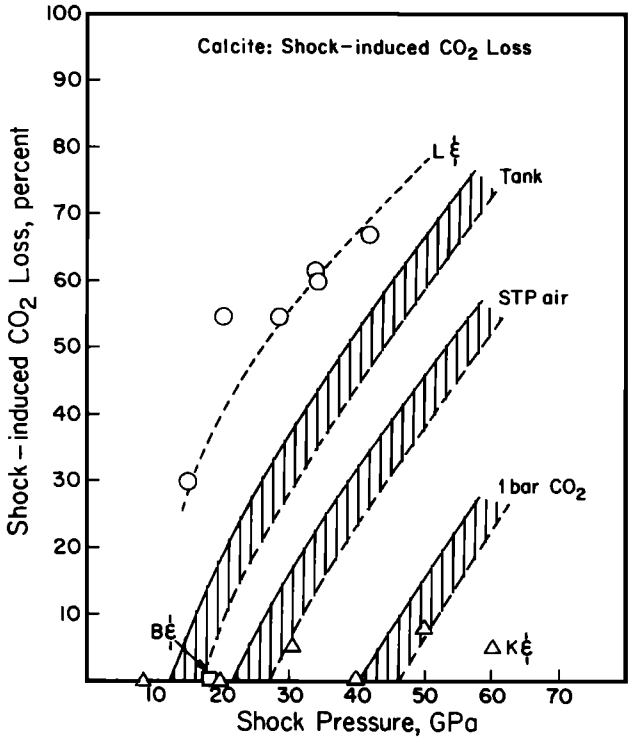

Fig. 13. Shock-induced CO_2 loss as a function of peak shock pressure in experimentally shock loaded single crystal calcite. Circles, Lange and Ahrens [1983]; square, Boslough et al. [1982]; triangles, Kotra et al. [1983]. Also shown are CO_2 losses calculated using shock entropy method for various values of ambient CO_2 pressure. "Tank" refers to the ambient CO_2 pressure in impact tank, about 4.3 x 10^{-8} bars; "STP air" refers to the P_{CO_2} in dry air at standard temperature and pressure conditions, about 3.3 x 10^{-4} bars; Solid lines refer to the following combination of parameters of calcite VI; ρ_o = 3.1 g/cm^3, K_{os} = 95 GPa, K' = 3.5, E_{trans} = 20 J/g. For dashed lines, ρ_o = 3.0 g/cm^3, K_{os} = 75 GPa, K' = 4.1, E_{trans} = 200 J/g.

$$\Delta G_{rx} = \Delta G^{\circ}_{rx} + RT\, ln\, P_{CO_2} \qquad (27)$$

where the reference state for the solids is defined as pure solids at 1 bar pressure and the temperature of interest T, and for CO_2 the reference state is pure CO_2 gas at 1 bar (10^5 Pa) pressure and T. Thus for P_{CO_2} = 1 bar the temperature of incipient vaporization T_{IV} is approximately 1171 K and the energy of incipient vaporization E_{IV}, given by

$$E_{IV} = \int_{T_o}^{T_{IV}} C_{v\,(calcite)}\, dT \qquad (28)$$

is approximately 980 J/g [Vizgirda and Ahrens, 1982; Kieffer and Simonds, 1980]. However, for $P_{CO_2} \sim 3.3x10^{-4}$ bar (corresponding to dry air at 1 bar total pressure) T_{IV} is approximately 800 K, and E_{IV} is about 530 J/g, and for $P_{CO_2} \sim 4.3x10^{-8}$ bar (corresponding to dry air at a total presure of 100 μm Hg) ,T_{IV} is about 596 K and E_{IV} is 296 J/g. Thus E_{IV} is strongly dependent on the explicit value of P_{CO_2} used in the calculation of T_{IV}, and conversely, the amount of CO_2 evolved during release may depend on the ambient P_{CO_2}.

Previous applications of shock energy and entropy caculations to mineral devolatilization have implicitly (and arbitrarily) assumed that the partial pressure of the volatile species is equal to 1 bar [Ahrens and O'Keefe, 1972; Kieffer and Simonds, 1980; Vizgirda and Ahrens, 1982; Lange and Ahrens, 1982b]. Note that although E_{IV} (P_{CO_2}), E_{CV} (P_{CO_2}), S_{IV} (P_{CO_2}), and S_{CV} (P_{CO_2}) are precisely known for calcite I, in Figures 12 and 14 they are shown as ranges because of the ambiguity in whether it is actually calcite I, II, or III that decomposes upon release.

Such equilibrium considerations do not apply absolutely in a dynamic shock experiment, but evidence that ambient CO_2 pressure affects the amount of evolved CO_2 comes from consideration of the experimental details of the three studies of impact-induced volatilization of calcite cited earlier. Boslough et al. [1982] studied the evolution of CO_2 during shock compression of calcite by capturing the evolved gas in an initially evacuated, confined chamber. For a shock pressure of 18 GPa, only 0.03-0.3 % of the CO_2 was volatilized, and the final P_{CO_2} in the chamber at room temperature was between about $2.7x10^{-3}$ to $7.2x10^{-3}$ bars (M. Boslough, personal communication, 1984). For $P_{CO_2} = 6x10^{-3}$ bars, T_{IV} = 900 K and E_{IV} = 648 J/g. The studies of Lange and Ahrens [1983, and unpublished manuscript, 1985] were performed using vented assemblies [Lange and Ahrens, 1982b]; therefore the final P_{CO_2} was that of air, $3.4x10^{-4}$ bar. For $P_{CO_2} = 3.4x10^{-4}$ bar, T_{IV} = 800 K, and E_{IV} = 528 J/g. They found significant decarbonation; as much as 30% at pressures as low as 10 GPa (see Figure 13). The analytical method was different in each of the two sets of experiments; Boslough et al. determined the amount of CO_2 evolved, whereas Lange and Ahrens determined the amount of CO_2 remaining in the recovered solid material. Nonetheless, it appears that at least part of the difference in results may be attributed to differences in P_{CO_2}. The results of

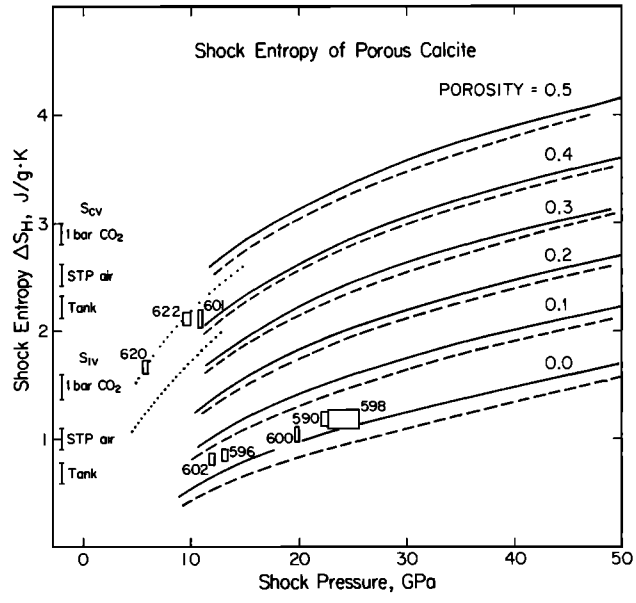

Fig. 14. Shock entropy as a function of shock pressure. The curves for porous calcite are calculated using the calcite Hugoniot of Adadurov et al. [1961] (Table 2), the correction for porosity embodied in equation (31), and the equation of state parameters for calcite VI listed in Table 3. S_{CV} and S_{IV} are calculated as a function of P_{CO_2} as described in text. Solid and dashed curves assume transformation to calcite VI; dotted curves assume no transformation, i.e., the low-pressure Hugoniot of calcite is employed (Table 2).

Kotra et al. [1983] differ from those discussed above because their targets (both vented and nonvented) were exposed to the CO_2-rich muzzle gases from the gun barrel. The very low fraction of CO_2 volatilized as a function of shock pressure obtained by these workers may be caused by very high P_{CO_2} during release.

There are several implications of these results.

1. The release paths determined in this study may not be completely comparable to the volatilization results of either Boslough et al. or Lange and Ahrens, inasmuch as the experiments reported here were performed at about 100 μm air pressure ($P_{CO_2} \sim 4.3 \times 10^{-8}$ bar). It is likely, however, that any differences would occur at release pressures lower than the lowest pressure for which we were able to obtain data.

2. The evolution of P_{CO_2} must be taken into account when calculating the evolution of impact-induced planetary atmospheric CO_2 content. Note also that these considerations apply to the shock entropy criterion for vaporization upon release [Ahrens and O'Keefe, 1972; Zel'dovich and Raizer, 1967] because this method also depends on the identification of a T_{IV} for calculation of S_{IV} (entropy of incipient vaporization). Furthermore, the equilibrium considerations apply to any shock devolatilization process, especially shock dehydration [cf. Boslough et al., 1980; Lange and Ahrens, 1982a, b].

Having demonstrated the consistency of experimental and theoretical postshock energy calculations, we now employ the postshock entropy method for further calculations of shock devolatilization of calcite [Zel'dovich and Raizer, 1967; Ahrens and O'Keefe, 1972]. This method uses the same parameters as the postshock energy method (i.e., K_o, K', ρ_o, and γ of the high-pressure polymorph, Table 3) and thus gives similar values for pressures of incipient devolatilization. It is, however, more convenient to use because it does not require or assume knowledge of the exact release path. Instead, the entropy gain in the shocked state ΔS_H is calculated according to

$$\Delta S_H = S_{tr} + C_v \ln (T_H/T_s) \quad (29)$$

where S_{tr} is the entropy of transition from calcite I to calcite VI at 1 bar and 298 K and T_H and T_s are calculated by continuum methods (equation (18) [Zel'dovich and Raizer, 1967]). The entropy of transition has been estimated to be between -0.116 and -0.086 J/g on the basis of entropy-molar volume systematics [Vizgirda and Ahrens, 1982] and we have adopted the value of -0.101 J/g for use here (Table 3). Note that Vizgirda and Ahrens [1982] apparently fail to include S_{tr} in the shock entropy calculations for calcite and aragonite. The shock entropy is dependent on T_H, which in turn is greatly influenced by the initial porosity of the material. Assuming isentropic release from the shocked state [Kieffer and Delaney, 1979; Jeanloz and Ahrens, 1979], and isentropic phase change upon release [Cowperthwaite and Ahrens, 1967], the entropy of the completely released state will be equal to that of the shocked state, and this value is compared to the entropy of incipient vaporization S_{IV}, where

$$S_{IV} = \int_{T_o}^{T_{IV}} \frac{C_p}{T} dT \quad (30)$$

where C_p is the atmospheric pressure heat capacity at constant pressure [Robie et al., 1978]. As discussed above, T_{IV} will be dependent on the P_{CO_2} chosen. The entropy of complete vaporization at T_{IV}, S_{cv}, is computed from the values of entropy as a function of temperature of Robie et al. [1978]. Figure 13 compares the impact-induced volatile loss at several values of P_{CO_2}, calculated using the shock entropy method, with the existing experimental data. The data of Boslough et al. [1982] and Kotra et al. [1983] are consistent with having been obtained at elevated CO_2 pressures. The results of Lange and Ahrens [1983] were obtained at STP. The agreement between the STP calculation and the data is improved over the calculation assuming P_{CO_2} equal to 1 bar, and the general shapes of the curves are similar. This suggests that the process modeled in the calculations are important for impact-induced devolatilization. On the other hand, the substantial level of disagreement is, of course, a clear indication that some other process must also be considered (see below).

Figure 14 is a plot of shock entropy versus shock pressure for calcite of varying porosities calculated using the calcite Hugoniot of Adadurov et al. [1961] and the parameters for calcite VI listed in Table 3. The Hugoniots for the porous material are calculated according to

$$P_p = P_D \left\{1 - \frac{\gamma}{2}\left[\frac{V_{o,D}}{V_H} - 1\right]\right\} \Big/ \left\{1 - \frac{\gamma}{2}\left[\frac{V_{o,P}}{V_H} - 1\right]\right\} \quad (31)$$

where P_p and P_D are the pressures at volume V_H of the porous material and the dense material, respectively, γ is the Gruneisen parameter, and $V_{o,p}$ and $V_{o,D}$ are the zero-pressure volumes of the porous and dense materials, respectively [Zel'dovich and Raizer, 1967; Ahrens and O'Keefe, 1972]. The experimentally determined shock entropies from this study are also plotted. The results for the Solenhofen limestone (initial porosity about .04) indicate that S_{IV} for $P_{CO_2} = 4.3 \times 10^{-8}$ bar (dry air atmosphere at 100 μm Hg total pressure, the conditions of the particle velocity experiment) is reached at about 12-17 GPa, and that at about 25 GPa between 20-30% of the CO_2 would be volatilized. The results from the Dover chalk shots (initial porosity of 0.49) indicate that greater than 90% of the material would be decarbonated at 10 GPa shock pressure under the experimental conditions. For an air atmosphere ($P_{CO_2} = 3.3 \times 10^{-4}$ bar) the figure indicates a minimum pressure for incipient devolatilization of nonporous calcite of 21 to 32 GPa, compared with the experimental value of less than 10 GPa determined by Lange and Ahrens.

The shock energy or entropy criteria for incipient and complete vaporization when applied using the ambient vapor composition (as opposed, for example, to an arbitrary assumption of 1 bar pressure of the volatile species) yield the lowest values of E_{IV} or S_{IV} and thus predict the greatest amount of devolatilization consistent with equilibrium thermodynamics. We assume that the atmospheric reservoir is large and that the addition of volatile species from the sample does not affect $P_{volatile}$. Thus equilibrium thermodynamic considerations fail to describe the experimental results for Solenhofen limestone even when the most generous assumptions concerning the final state of equilibrium are made.

We therefore conclude that a mechanism for the localization of thermal energy such as the shear instability model [Grady, 1977, 1980; Horie, 1980] is required to explain the experimental observations. In the case of single crystal calcite the existing determinations of color temperature under shock support this conclusion. Kondo and Ahrens [1983] report a temperature of 3700 K and an emissivity of 0.0025 for single crystal calcite shocked to 40 GPa. This temperature is several times the continuum shock temperature of 1300-1500 K [Vizgirda and Ahrens, 1982]. Textural examination of recovered calcite shocked to 40 GPa suggests the presence of partially molten material into which shock released CO_2 has been injected [M. A. Lange and T. J. Ahrens, manuscript in preparation, 1985]. D. R. Schmitt (personal communication, 1984) has measured a color temperature of 2455 K for single-crystal calcite shocked to 22.5 GPa.

The relationships between measured shock tempera-

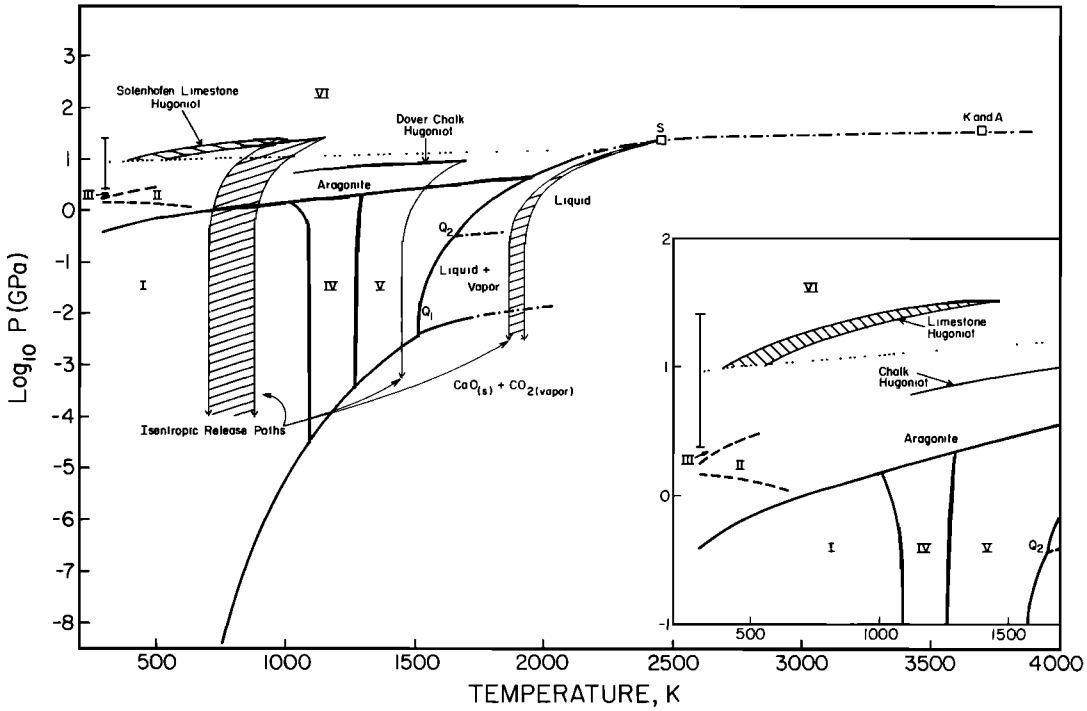

Fig. 15. $CaCO_3$ phase diagram showing schematic paths of isentropic decompression from shocked states. The PT phase diagram is based on the results of Carlson [1983], Huang and Wyllie [1976], Irving and Wyllie [1973], Baker [1962], and Jamieson [1957]. Stability fields of each polymorph are labeled with the appropriate roman numeral. The range of Hugoniot and release path temperatures for Solenhofen limestone are calculated using the range of values of properties of calcite VI (Table 3). Hugoniot and representative release path temperatures of Dover chalk are based on the low-pressure calcite properties (Table 3). Open squares are shear band color temperature measurements on single-crystal calcite by Kondo and Ahrens [1983] (K & A) and by D. R. Schmitt (personal communication, 1984) (S). These are interpreted as representing points on the fusion curve. The representative isentropic release path for the point S is calculated using the calcite VI physical property data. Note that 10^{-4} GPa corresponds to 1 bar pressure. Q_1 is the invariant point, at which $CaCO_{3(s)}$, $CaO_{(s)}$, $CO_{2(vapor)}$, and liquid coexist. $CaCO_3$ melts incongruently between points Q_1 and Q_2 and melts congruently at pressures higher than Q_2. Metastable calcite II and III fields are separated by dashed lines. Extrapolated or inferred phase boundaries are shown by dash-dot lines. Dotted line represents the aragonite $\rightleftarrows$ calcite VI phase boundary constrained to lie below the limestone Hugoniot. Error bar on the dotted line represents the position of the line calculated using the range of property values for calcite VI listed in Table 3.

tures, calculated continuum temperatures, release paths, and the calcite devolatilization equilibria are shown in Figure 15. Figure 15 shows the PT phase diagram for $CaCO_3$, the Hugoniot (continuum) PT data for the Solenhofen limestone and Dover chalk reported here, and the measured shock temperatures of single-crystal calcite of D. R. Schmitt (personal communication, 1984) and Kondo and Ahrens [1983]. The calcite VI-liquid boundary is drawn through the two measured shock temperature values, but the conclusions drawn below do not depend critically on this particular placement of the boundary. Representative isentropic release paths, using the parameters in Table 3, are shown for several points. The diagram illustrates that the isentropic release paths of shocked nonporous carbonates (Solenhofen limestone), calculated using continuum temperatures, do not cross into the $CaO_{(s)} + CO_{2\,(vapor)}$ field until very low pressures (10^{-7} – 10^{-8} GPa) are reached. Shocked Dover chalk, particularly at shock pressures as high as 10 GPa, relaxes into the solid plus vapor region at pressures of 10^{-3} to 10^{-4} GPa. However, isentropic release from points corresponding to measured shock temperatures pass into the liquid field region at pressures of 10^{1} GPa or higher, into the liquid plus vapor field at pressures of 10^{-1} GPa or higher, and then into the solid plus vapor region at pressures of about 10^{-2} GPa. The high measured shock temperatures are related to shear banding phenomena, and it thus appears that localization of thermal energy is an integral part of the devolatilization process. The diagram also indicates that the effect of CO_2 pressure on the fraction devolatilized will be more modest in the case of shear band controlled devolatilization than in the case of devolatilization controlled by continuum temperatures.

Conclusions

Solenhofen limestone shocked into the calcite VI region retains its shear strength in the shocked state at pressures between about 12 and 20 GPa. Equilibrium thermodynamic calculation of the energy and entropy required for incipient devolatilization combined with calculated values of the postshock energy and entropy gain fail to predict quantitatively the amount of volatile loss upon release. This result indicates that inhomogeneous deformation processes occur in this pressure range. The shear bands may be sites of initiation of partial melting and nucleation of evolved CO_2 upon release. Therefore the density of the

shear bands created in this shock-pressure interval must be insufficient to modify the bulk mechanical properties of the polycrystalline aggregate. At shock pressures above about 20 GPa loss of strength of the material may occur, implying that the shear band density is large enough to affect mechanical properties. These shear band related phenomena occur in a shock pressure range in which no solid-solid phase transitions are observed. Isentropic release paths of material initially at the shock pressure and the measured shock temperature pass through the vapor plus liquid field into the vapor plus solid field, giving further support to the concept that devolatilization is associated with shear band formation.

At shock pressures of about 10 GPa, Dover chalk ($\rho_o = 1.40$ g/cm^3) appears to have lost its shear strength, but at 5 GPa the results are ambiguous. Postshock entropy calculations indicate that greater than 90% of the CO_2 is devolatilized upon release from 10 GPa pressure.

Equilibrium calculations and experimental observations indicate that the amount of devolatilization of volatile-bearing minerals upon impact is dependent on the ambient partial pressure of the volatile species. The shock pressure required for incipient devolatilization increases with ambient volatile species partial pressure. This effect causes the range of planet sizes in which partial devolatilization of carbonates occurs to be larger than that calculated based on devolatilization experiments carried out in air [Lange and Ahrens, 1983, and unpublished manuscript, 1985]. Volatile release is enhanced relative to that calculated by Lange and Ahrens in the early stages of planetary accretion, when the atmosphere is sparse, and is inhibited in the later stages, when the atmosphere is relatively dense.

Acknowledgments. We thank E. Gelle, M. Long, W. Miller, and C. Manning for their help in performing these experiments. M. Boslough, S. Rigden, and B. Svendsen provided valuable insight and discussion. The comments of anonymous reviewers helped improve the manuscript. Research supported by NASA NGL-05-002-105. Contribution 4134, Division of Geological and Planetary Sciences, California Institute of Technology.

References

Adadurov, G. A. D., D. B. Balashov, and A. N. Dremin, A study of the volumetric compressibility of marble at high pressures, Bull. Acad. Sci. USSR Geophys. Ser., 1961(5), 463-466, 1961.

Ahrens, T. J., and V. G. Gregson, Jr., Shock compression of crustal rocks: Data for quartz, calcite, and plagioclase rocks, J. Geophys. Res., 69, 4839-4874, 1964.

Ahrens, T. J., and J. D. O'Keefe, Shock melting and vaporization of lunar rocks and minerals, Moon, 4, 214-249, 1972.

Ahrens, T. J., and J. T. Rosenberg, Shock Metamorphism: Experiments on quartz and plagioclase, in Shock Metamorphism of Natural Materials, edited by B. M. French and N. M. Short, pp. 59-81, Mono, Baltimore, Md., 1968.

Ahrens, T. J., J. L. Lower, and P. L. Lagus, Equation of state of forsterite, J. Geophys. Res., 76, 518-528, 1971.

Anderson, O. L., E. Schreiber, and R. C. Liebermann, Some elastic constant data on minerals relevant to geophysics, Rev. Geophys., 6, 491-524, 1968.

Baker, E. H., The calcium oxide-carbon dioxide system in the pressure range 1-300 atmospheres, Chem. Soc. J., 1962, 464-470, 1962.

Bless, S. J., and T. J. Ahrens, Measurement of release wave speed in shock compressed polycrystalline alumina and aluminum, J. Geophys. Res., 81, 1935-1942, 1976.

Boslough, M. B., Shock-wave properties and high-pressure equations of state of geophysically important materials, Ph.D. thesis, Calif. Inst. of Technol., Pasadena, 1983.

Boslough, M. B., and T. J. Ahrens, Shock wave properties of anorthosite and gabbro, J. Geophys. Res., 90, 7814-7820, 1985.

Boslough, M. B., R. J. Weldon, and T. J. Ahrens, Impact-induced water loss from serpentine, nontronite, and kernite, Proc. Lunar Planet. Sci. Conf., 11th, 2145-2158, 1980.

Boslough, M. B., T. J. Ahrens, J. Vizgirda, R. H. Becker, and S. Epstein, Shock-induced devolatilization of calcite, Earth Planet. Sci. Lett., 61, 166-170, 1982.

Bottinga, Y., and P. Richet, High pressure and temperature equation of state and calculation of the thermodynamic properties of gaseous carbon dioxide, Am. J. Sci., 281, 615-660, 1981.

Bridgman, P. W., The high pressure behavior of miscellaneous minerals, Am. J. Sci., 237, 7-18, 1939.

Burdick, L., and D. L. Anderson, Interpretation of velocity profiles of the mantle, J. Geophys. Res., 80, 1070-1074, 1975.

Carlson, W. D., The polymorphs of $CaCO_3$ and the aragonite-calcite transformation, in Carbonates: Mineralogy and Chemistry, Rev. Mineral., vol. 11, edited by R. J. Reeder, pp. 191-225, Mineralogical Society of America, Washington, D. C., 1983.

Courant, R., and K. O. Friedrichs, Supersonic Flow and Shock Waves, Wiley-Interscience, New York, 1948.

Cowperthwaite, M., and T. J. Ahrens, Thermodynamics of the adiabatic expansion of a mixture of two phases, Am. J. Phys., 35, 951-955, 1967.

Cowperthwaite, M., and R. F. Williams, Determination of constitutive relationships with multiple gauges in nondivergent flow, J. Appl. Phys., 42, 456-462, 1971.

Grady, D. E., Processes occurring in shock wave compression of rocks and minerals, in High Pressure Research: Applications in Geophysics, edited by M. H. Manghnani and S. Akimoto, pp. 389-438, Academic, Orlando, Fla., 1977.

Grady, D. E., Interrelation of flow or fracture and phase transition in the deformation of carbonate rock, J. Geophys. Res., 84, 7549-7554, 1979.

Grady, D. E., Shock deformation of brittle solids, J. Geophys. Res., 85, 913-924, 1980.

Grady, D. E., Compression wave studies in Oakhall Limestone, Rep. SAND83-0370, Sandia Natl. Lab., Albuquerque, N. M., 1983.

Grady, D. E., and R. L. Moody, Shock and release equation of state of calcite, Rep. SAND85-0947, Sandia Natl. Lab., Albuquerque, N. M., 1985.

Grady, D. E., W. I. Murri, and G. R. Fowles, Quartz to stishovite: Wave propagation in the mixed phase region, J. Geophys. Res., 79, 332-338, 1974.

Grady, D. E., W. I. Murri, and P. S. DeCarli, Hugoniot sound velocities and phase transformations in two silicates, J. Geophys. Res., 80, 4857-4861, 1975.

Grady, D. E., R. E. Hollenbach, K. W. Schuler, and J. F. Callender, Compression wave studies in Blair dolomite, Rep. SAND 76-0005, Sandia Natl. Lab., Albuquerque, N. M., 1976.

Grady, D. E., R. E. Hollenbach, and K. W. Schuler, Compression wave studies on calcite rock, J. Geophys. Res., 83, 2839-2849, 1978.

Grieve, R. A. F., and P. B. Robertson, The terrestrial cratering record, 1, Current status of observations, Icarus, 83, 212-229, 1979.

Horie, Y., Thermodynamics of dislocations and shock compression of solids, Phys. Rev. B Condens. Matter, 21, 5549-5557, 1980.

Huang, W.-L., and P. J. Wyllie, Melting relations in the systems CaO-CO_2 and MgO-CO_2 to 33 kilobars, Geochim. Cosmochim. Acta, 40, 129-132, 1976.

Hughes, D. S., and J. H. Cross, Elastic wave velocities in

rocks at high pressures and temperatures, Geophysics, 16, 577-593, 1951.
Irving, A. J., and P. J. Wyllie, Melting relationships in $CaO-CO_2$ and $MgO-CO_2$ to 36 kilobars with comments on CO_2 in the mantle, Earth Planet. Sci. Lett., 20, 220-225, 1973.
Jamieson, J. C., Introductory studies of high-pressure polymorphism to 24,000 bars by x-ray diffraction with some comments on calcite II, J. Geol., 65, 334-343, 1957.
Jeanloz, R., and T. J. Ahrens, Release adiabat measurements on minerals: The effect of viscosity, J. Geophys. Res., 84, 7545-7548, 1979.
Jeanloz, R., and T. J. Ahrens, Equations of state of FeO and CaO, Geophys. J. R. Astron. Soc., 62, 505-528, 1980.
Kalashnikov, N. G., M. N. Pavlovskiy, G. V. Simakov, and R. F. Trunin, Dynamic compressibility of calcite-group minerals, Izv. Acad. Sci. USSR Phys. Solid Earth, Engl. Transl. 1973(2), 80-84, 1973.
Kerrick, D. M., and G. K. Jacobs, A modified Redlich-Kwong equation for H_2O, CO_2, and H_2O-CO_2 mixtures at elevated pressures and temperatures, Am. J. Sci., 281, 735-767, 1981.
Kieffer, S. W., and J. W. Delaney, Isentropic decompression of fluids from crustal and mantle pressures, J. Geophys. Res., 84, 1611-1620, 1979.
Kieffer, S. W., and C. H. Simonds, The role of volatiles and lithology in the impact cratering process, Rev. Geophys., 18, 143-181, 1980.
Kondo, K., and T. J. Ahrens, Heterogeneous shock-induced thermal radiation in minerals, Phys. Chem. Miner., 9, 173-181, 1983.
Kotra, R. K., T. H. See, E. K. Gibson, F. Horz, M. J. Cintala, and R. S. Schmidt, Carbon dioxide loss in experimentally shocked calcite and limestone, Lunar Planet. Sci., 14, 401-402, 1983.
Lange, M. A., and T. J. Ahrens, The evolution of an impact generated atmosphere, Icarus, 51, 96-120, 1982a.
Lange, M. A., and T. J. Ahrens, Impact induced dehydration of serpentine and the evolution of planetary atmospheres, Proc. Lunar Planet. Sci. Conf. 13th, part 1, J. Geophys. Res., 87, suppl., A451-A456, 1982b.
Lange, M. A., and T. J. Ahrens, Shock-induced CO_2 production from carbonates and a proto-CO_2 atmosphere on the Earth, Lunar Planet. Sci., 14, 419-420, 1983.
Larson, D. B., and G. D. Anderson, Plane shock wave studies of porous geologic media, J. Geophys. Res., 84, 4592-4600, 1979.
Marsh, S. P. (Ed.), LASL Shock Hugoniot Data, University of California Press, Berkeley, 1980.
McQueen, R. G., S. P. Marsh, and J. N. Fritz, Hugoniot equation of state of twelve rocks, J. Geophys. Res., 72, 4999-5036, 1967.
McQueen, R. G., S. P. Marsh, J. W. Taylor, J. N. Fritz, and W. J. Carter, The equation of state of solids from shock wave studies, in High-Velocity Impact Phenomena, edited by R. Kinslow, pp. 293-417, Academic, Orlando, Fla., 1970.
Murri, W. J., D. E. Grady, and K. D. Mahrer, Equation of state of rocks, Final Rep. PYU-1883, Stanford Res. Inst., Menlo Park, Calif., 1975.
Peselnick, L., Elastic constants of Solenhofen limestone and their dependence on density and saturation, J. Geophys. Res., 67, 4441-4448, 1962.
Peselnick, L., and W. H. Wilson, Wave velocities and hysteresis in Solenhofen limestone for pressures up to 12 kilobars, J. Geophys. Res., 73, 3271-3280, 1968.
Petersen, C. F., W. J. Murri, and M. Cowperthwaite, Hugoniot and release-adiabat measurements for selected geologic materials, J. Geophys. Res., 75, 2063-2072, 1970.
Robie, R. A., B. S. Hemingway, and J. R. Fisher, Thermodynamic properties of minerals and related substances at 298.15K and 1 bar (10^5 pascals) pressure and at higher temperatures, U.S. Geol. Surv. Bull., 1452, 1978.
Sammis, C., D. L. Anderson, and T. Jordan, Application of isotropic finite strain theory to ultrasonic and seismological data, J. Geophys. Res., 75, 4478-4480, 1970.
Schuler, K. W., and D. E. Grady, Compression wave studies in Solenhofen Limestone, Rep. SAND76-0279, Sandia Natl. Lab., Albuquerque, N. M., 1977.
Singh, A. K., and G. C. Kennedy, Compression of calcite to 40 kbar, J. Geophys. Res., 79, 2615-2622, 1974.
van Thiel, M., J. Shaner, and E. Salinas, Rep. UCRL 50108, vol. 3, Lawrence Livermore Lab., Livermore, Calif., 1977.
Vizgirda, J., and T. J. Ahrens, Shock compression of aragonite and implications for the equation of state of carbonates, J. Geophys. Res., 87, 4747-4758, 1982.
Wang, C., and M. Meltzer, Propagation of sound waves in a rock undergoing phase transformations, J. Geophys. Res., 78, 1293-1298, 1973.
Zel'dovich, Ya., B., and Yu. P. Raizer, Physics of Shock Waves and High-Temperature Hydrodynamic Phenomena, vol. II, Academic, Orlando, Fla., 1967.

J. A. Tyburczy and T. J. Ahrens, Seismological Laboratory, California Institute of Technology, MA/252-21, 1201 E. California Blvd., Pasadena, CA 91125.

(Received November 26, 1984;
revised August 5, 1985;
accepted August 9, 1985.)